JOURNAL OF PROPULSION AND POWER
Vol. 16, No. 3, May–June 2000

Experiment to Support the Formulation and Validation of Compressor-Face Boundary Conditions

Donald Freund*
Gulfstream Aerospace Corporation, Savannah, Georgia 31402-2206
and
Miklos Sajben†
University of Cincinnati, Cincinnati, Ohio 45221-0070

The reliability of unsteady inlet flow computations may be seriously degraded by the lack of experimentally validated compressor-face (outflow) boundary conditions. The commonly imposed outflow conditions require a flow variable to be constant (pressure, velocity, Mach number, etc.) at the outflow boundary, but there is little if any documented evidence to support these assumptions, nor are they likely to actually occur during a rapid transient of a real inlet/engine system. Measurements are presented of acoustic reflection coefficients for an operating multistage compressor, a quantity appropriate for the characterization of the compressor face for computational purposes. The experiment used an impulse method, in which short-duration, large-amplitude acoustic pulses (1 ms, with a peak value of nearly 4% of the mean static pressure, respectively) were generated in a constant-area, annular inlet. The pulse and its reflection from the compressor face were tracked by fast-response pressure transducers. Frequency-domain analysis of the data yields transfer functions that may be thought of as frequency-resolved reflection coefficients. None of the currently available compressor-face boundary conditions accurately predict the data obtained in this study, indicating that current practices concerning outflow boundary conditions are in need of revision.

Nomenclature

a	= sound speed, m/s
d	= diameter, m
f	= frequency, Hz
$H[f]$	= transfer function
h	= annulus height, m
M	= axial Mach number
p	= static pressure, Pa
q	= dynamic pressure, Pa
$R[f]$	= magnitude of transfer function
t	= time, s
x	= axial location; zero at axial midpoint of first stage rotor, positive in downstream direction, m
$Y[f]$	= Fourier transform of input time history
$Z[f]$	= Fourier transform of output time history
Γ	= Variable inlet guide vane stagger angle, deg
$\xi[f]$	= reflection location, m
$\tau[f]$	= time delay, s
$\phi[f]$	= phase angle, rad

Subscripts

c	= inlet case
0	= undisturbed value

Superscripts

$'$	= perturbation value
~	= scaled parameter

Introduction

AN important issue in both the NASA High-Speed Research and High-Speed Civil Transport (HSCT) programs is the stability of supersonic, mixed compression inlets. The design cruise speed of the proposed HSCT aircraft is Mach 2.4, and at this speed mixed compression inlets offer better pressure recovery and lower cowl drag than external compression inlets. However, mixed compression inlets are susceptible to an undesirable transient process, called unstart, that results in the expulsion of the terminal shock structure from the inlet. Inlet unstart may be initiated by abrupt changes in freestream conditions, e.g., pressure, temperature, incidence angle, etc., engine generated disturbances, e.g., compressor surge, afterburner transient, etc., or control surface generated vortical disturbances. An unstart can reduce the inlet pressure recovery and inlet mass flow by as much as 50%, which could initiate a compressor stall or surge, leading to a possible engine flameout.[1] In addition, the disgorged shock can also disturb the wing boundary layers and cause major changes in lift and drag. An engine flameout coupled with high spillage drag would require large control surface deflections to overcome the asymmetric loading on the aircraft. The abrupt vehicle movements associated with an unstart are undesirable for any aircraft and probably unacceptable for supersonic commercial transports, i.e., HSCT.[2]

Because full-scale (ground or flight) testing is enormously expensive, unstart prediction is generally addressed using computational fluid dynamics (CFD).[3–10] The modeling of joint inlet/compressor systems has been accomplished, but only at the expense of describing the compressor with one-dimensional models.[3,11,12] Because inlet/compressor studies including a high-fidelity modeling of the compressor are not currently practical, the inlet flows are usually computed separately, with the compressor dynamics represented by an outflow boundary condition.

Until quite recently, the most common practice has been to set a selected variable constant at the outflow boundary of the inlet. The variable may be chosen as axial velocity,[3] axial Mach number,[4,5] static pressure,[3–5] or corrected mass flow.[8] Chung and Cole[5] proposed a uniform Mach number at the compressor face while allowing a radial variation in static pressure, which is updated based on the upstream conditions. All of these boundary conditions were selected on the basis of intuitive arguments and/or mathematical convenience. Most of these boundary conditions are straightforward extensions of practices that are valid for and work well with steady inlet flows.

Received 26 June 1998; revision received 5 February 1999; accepted for publication 15 April 1999.

*Engineer, Flight Sciences; don_freund@gulfaero.com. Member AIAA.
†Professor, Department of Aerospace Engineering and Engineering Mechanics; m.sajben@uc.edu. Fellow AIAA.

A literature search into unsteady supersonic inlet and/or compressor behavior could locate no experimental justification for the currently implemented compressor-face boundary conditions in an unsteady situation. There has been much work on unstart,[13,14] control system-induced transients,[15–17] dynamic inlet distortion,[18–20] hammershock,[21,22] and inlet buzz.[23] These references are samples from a large number of publications. However, there are no data that can be used to validate the currently customary boundary conditions or formulate new ones.

Disturbances

In the present work, disturbances are characterized following Kovasznay,[24] who has shown that disturbances associated with the turbulent motion of a compressible fluid may be decomposed into three modes of fluctuations: vorticity, acoustic, and entropy modes. If the disturbance scales are sufficiently small and the mean flow is uniform, then each of these modes is governed by an independent equation. The acoustic mode is described by a wave equation. The other two are convected with the flow, while subject to molecular diffusion. For the short-duration events considered here, diffusion is negligible, and convection is the primary mechanism. If the amplitudes are large, then the modes interact to a degree that increases with the disturbance amplitudes, and the decomposition may not be unique.

It is relatively easy to create nearly pure acoustic, vortical, or entropy disturbances experimentally. It is expected that it will be possible to establish a correspondence between experiment and theory if both avenues of work are focused on such single-mode disturbances.

Acoustic (pressure) disturbances were selected on the basis that they are the easiest to generate and are readily detected with pressure transducers. In addition, acoustic disturbances propagate at speeds very different from the mean flow velocity and are easily differentiated from vorticity and entropy disturbances, both of which convect at the flow speed.

Various types of acoustic disturbances were considered: periodic,[20,25,26] step changes, and short-duration pulses. For experimental convenience and clarity of data interpretation, the type eventually chosen was a solitary pulse approximating a delta function: a momentary change in pressure with as short a duration as possible. The reflection generated by the pulse will depend entirely on the processes occurring at the compressor.

Analytical and Computational Studies of the Acoustic Reflection Process

Kaji and Okazaki,[27,28] were the first to analytically investigate the propagation of planar sound waves through a cascade, using the semiactuator disk theory and the acceleration potential method. Their results show that the stagger angle of the cascade has the greatest impact on the amplitude of the reflection, whereas the axial Mach number and solidity were shown to be secondary in nature. The effect of blade loading was also investigated and found to be negligible.

In-depth studies of the reflection process were published by Paynter,[29,30] who computed the response of two-dimensional cascades to acoustic disturbances arriving from upstream and developed an analytical reflection model. His results show that the amplitude of the reflected pulse strongly depends on the cascade stagger angle and the axial Mach number. Paynter also found that the influence of the incident pulse strength, blade loading, and solidity were minor.

These analytical and computational results illustrate the clear need for boundary conditions that have been experimentally demonstrated to be acceptable representations of compressor dynamics during transient processes. This paper documents the experimental determination of the short-time response of a compressor to short-duration, planar pressure pulses arriving to the compressor from upstream. The data are suitable for the formulation and validation of compressor-face boundary conditions for unsteady inlet flow computations. It is believed that this is the first published data set focused on the dynamic characteristics of a compressor-face. Extensive details of the project may be found in Refs. 31–35.

Concept of the Experiment

The experiment was carried out in a facility consisting of a constant-area annular inlet with a General Electric T58 helicopter engine (Fig. 1). A pulse generator is located near the midpoint of the inlet. Activation of the generator creates a pair of acoustic pulses, one propagating upstream and one propagating downstream. The processes are shown in the $x-t$ diagram of Fig. 2. The downstream moving pulses are labeled as D1, D2, etc., whereas the upstream moving pulses are U1, U2, etc., in the order of appearance. Upon reaching the ends of the inlet, reflections are generated that traverse the inlet in the opposite directions. The D1 → U2 reflection is of principal interest. The diagram shows that the pulses are of finite duration, which has a significant impact on the data interpretation process.

The constant-area duct obviously does not simulate a real inlet, but this is not necessary because the interest is focused solely on the outflow boundary. The constant area keeps the mean flow well behaved and leads to pulses that propagate without changing their structure or speed. These properties are critical for a simple but accurate interpretation of the data.

Attention is focused on the reflection process occurring at the compressor face. If the incident and reflected pulses to and from the

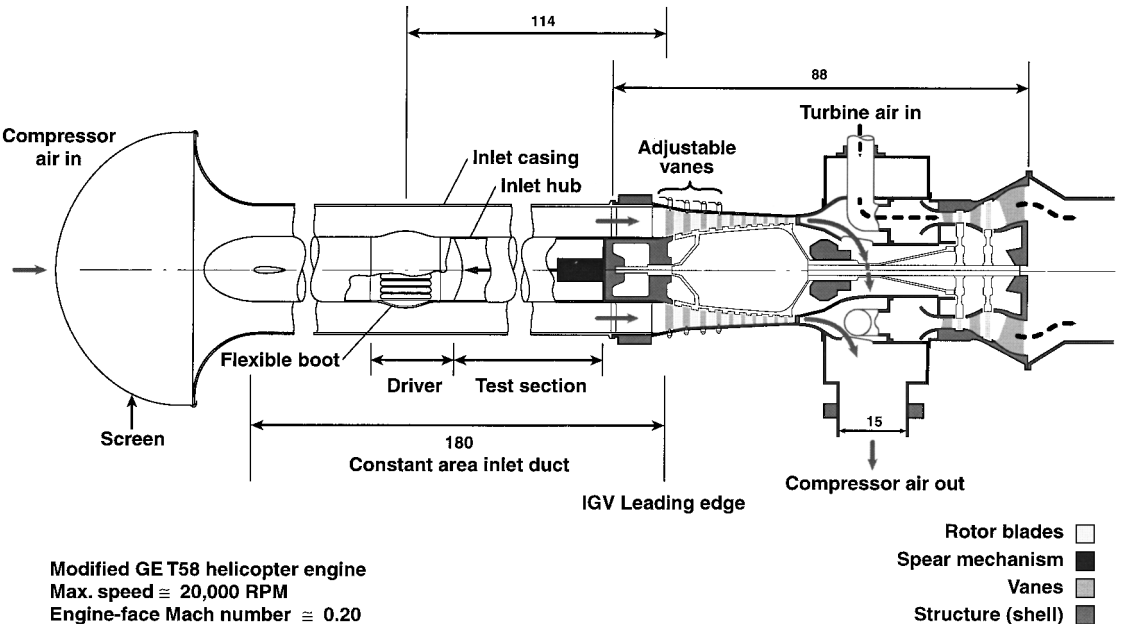

Fig. 1 Inlet duct and compressor rig, all dimensions in centimeters.

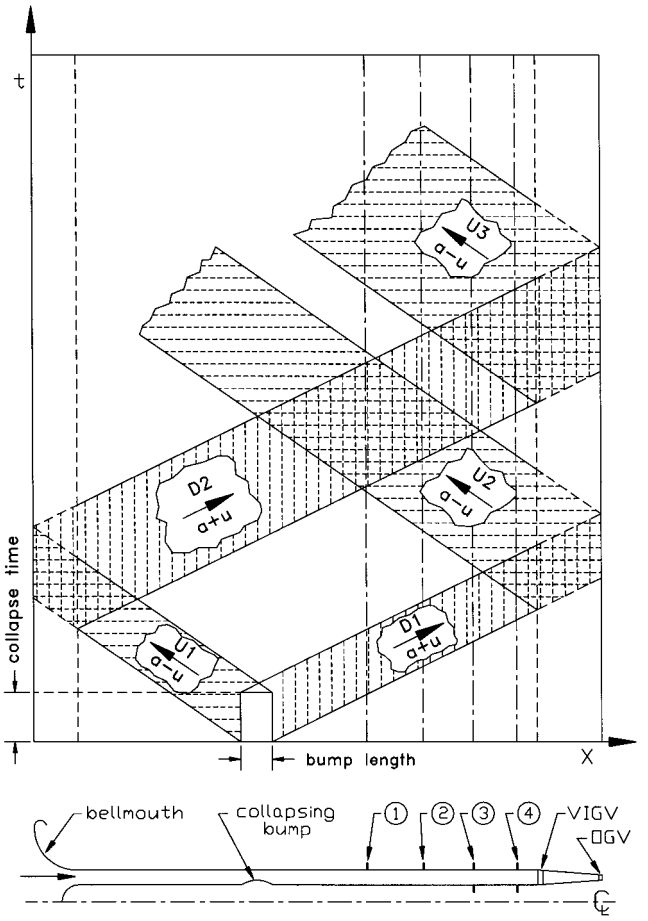

Fig. 2 Dynamic processes initiated by the bump collapse, x–t diagram.

compressor are sufficiently short to be separable from reflections generated at the bellmouth, then their respective structures can be determined accurately. Once the pressure–time histories for both the incident and reflected pulses are available, the reflection process can be characterized by appropriate methods.

Experimental Facilities

The compressor facility (Fig. 1) is a General Electric T58-3 helicopter engine, with the power turbine removed. The engine has been modified for cold operation in that the combustor and fuel injection systems have been removed and replaced with a plenum chamber that supplies the turbine with high-pressure air from an external source. Because the enthalpy of the air supplied to the turbine is much less than that in a normally operating engine, the maximum attainable speed is 20,000 rpm (76% of design, 26,300 rpm) with a corresponding compressor-face axial Mach number of 0.18. Turbine airflow rates of 7 kg/s (15 lbm/s) are typical at 20,000 rpm. The engine speed is controlled by varying the stagnation pressure to the turbine inlet. Speed could be set and held within ±50 rpm using a dedicated proportional integral derivative controller.

The compressor has 10 stages and a design pressure ratio of 8.2. The compressor exhausts to the atmosphere through an orifice plate sized to achieve the desired compressor pressure ratio (in most cases slightly below the operating line), which varied up to 2.7 in these experiments.

The compressor has a variable inlet guide vane (VIGV) row and the second through fourth stages also have variable stator vanes. The four variable vane rows are gang controlled with a linear actuator that can be moved independently of the other engine parameters. There are 38 uncambered VIGVs, whose stagger angle Γ is variable from 31.7 to −5.3 deg (0 deg corresponds to wide open). Solidity (chord/spacing ratio) at the mean diameter of the VIGV is 1.2.

The first stage rotor has 30 blades, with a tip diameter of 0.247 m, and the mean-diameter solidity and stagger angle are 1.16 and 52 deg, respectively. The front rotor bearing is supported by four struts, located just upstream of the VIGVs. The struts have streamlined shapes, with a streamwise length of 0.07 m, and represent a 9.2% blockage of the annulus area. The axial centerline of the first-stage rotor was selected as the origin for the x axis, with positive values in the direction of the flow, i.e., into the engine. Angular position is specified by the polar angle θ, where $\theta = 0$ deg at the 12 o'clock position and is positive clockwise when looking downstream.

The blade configuration data for the T58 compressor is considered proprietary information by the General Electric Company (GE), and the detailed specifications for the compressor blade rows cannot be included.

Figure 1 shows the compressor rig mated with a constant-area annular inlet duct. The length of the constant-area duct segment is 180 cm (71 in.), and the hub/casing diameters of the annulus are 13.7/25.8 cm (5.38/10.17 in.). The air enters through a screened bellmouth intended to remove steady or unsteady distortions that might originate from the environment. The hub contains a mechanism capable of generating individual acoustic pulses. The pulse generator design is based on a novel concept, whose design and performance are described in Refs. 31–33. Only a brief description is included here.

As shown in Fig. 2, the downstream moving wave (D1 pulse) is used to study the reflection process. The D1 pulse is a 1-ms-duration expansion wave with typical magnitude of 4% of the mean static pressure, generated with a high degree of repeatability. The pulse is followed by several cycles of ringing at 1.5 kHz at a much smaller amplitude. Because the pulse is generated by the radial movement of the boundary, there are also radial modes present at about 3 kHz. The radial modes were shown to decay, and the pulse arriving at the compressor face is nearly planar.

The D1 pulse shape remains essentially constant during propagation; hence, the pulse is a fixed spatial pattern translating downstream without significant attenuation or diffusion (this is to be expected due to the short distances involved). In addition, the pulse speed is accurately equal to $a_0 + u_0$ of sound as seen in the laboratory frame of reference. These pulse characteristics were found apply to all runs, which greatly simplified the interpretation of the data.

Results: Time Mean Flow

The axial static pressure distribution in the inlet was measured with 65 wall taps on the inlet case spanning from downstream of the bellmouth to just upstream of the VIGVs. The taps were connected to a scanivalve multiport transducer with the output recorded with a personal computer-controlled, 16-bit, data acquisition board (resolution approximately equal to 2 Pa). The axial pressure distribution in the inlet was shown to be nearly linear, except for minor depressions in the vicinity of the inlet struts and compressor front frame struts, as a result of the localized reduction in the annulus cross-sectional area. The linear pressure distribution is representative of a well-behaved turbulent flow in the inlet.

There were additional taps located about the case perimeter just downstream of the bellmouth, over the pulse generator, and upstream of the VIGVs. The deviations observed at each axial station were on the order of 1% of q_0.

The uniformity of the inlet flow just downstream of the bellmouth was determined with a translating pitot probe rake. Velocity profiles taken at four circumferential positions (relative circumferential spacing is 90 deg) were found to be circumferentially and radially uniform, except for the small hub and case boundary layers.

The static pressure and the velocity profile measurements indicate that the flow in the inlet is axisymmetric. Further details may be found in Ref. 31.

Results: Dynamic Data

Scaling

The wave propagation processes are dominated by inviscid mechanisms and can be scaled by choosing the appropriate normalization scheme. The required nondimensional variables are obtained

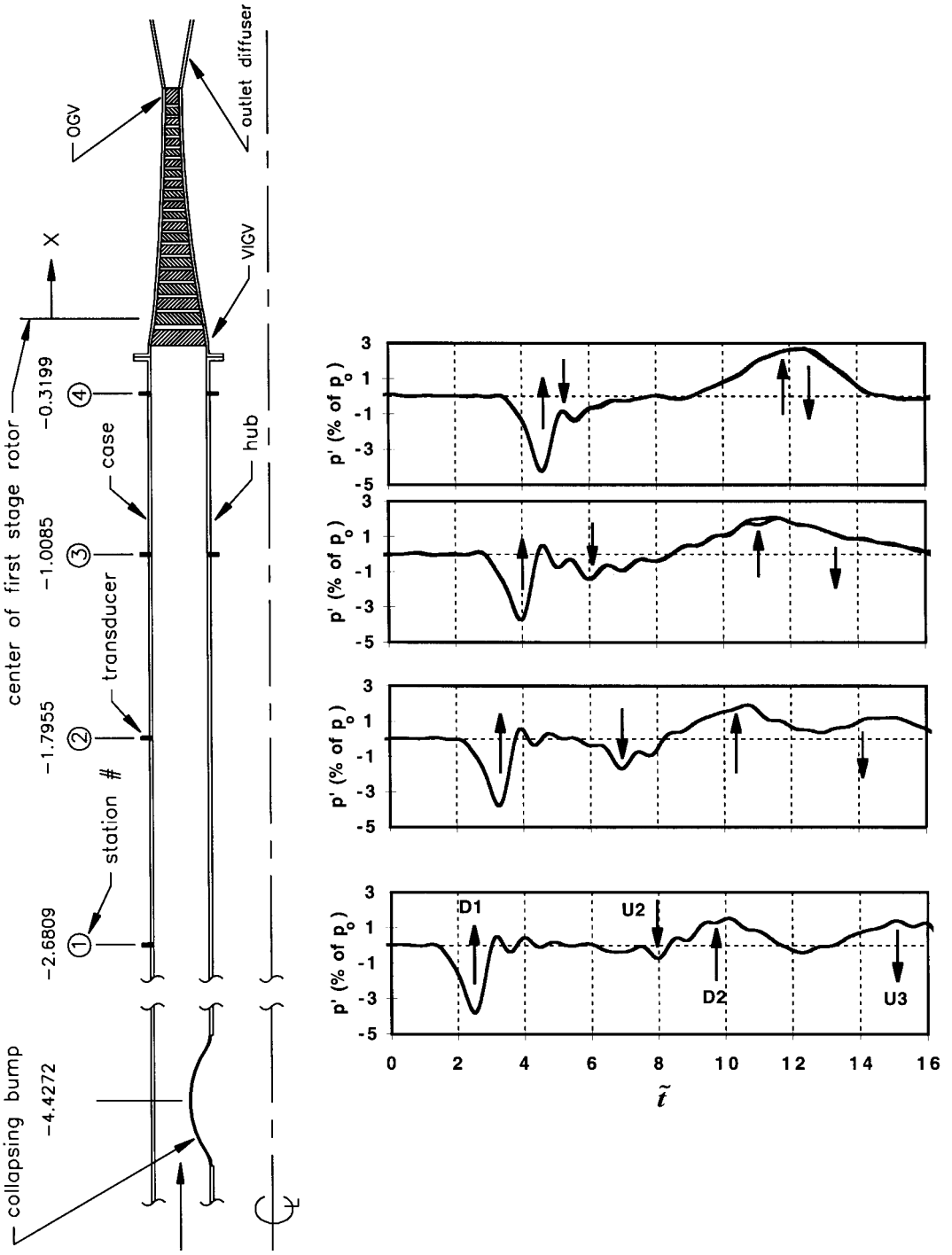

Fig. 3 Temporal evolution of static pressure in the inlet for $M_0 = 0.17$; vertical arrows indicate direction of propagation.

by nondimensionalizing the Euler equations. The results presented in this format can then be used for larger applications, e.g., HSCT inlet configuration, with a diameter at the compressor face in excess of 1 m. In addition, the scaled equations account for the small temperature differences between runs, which produce even smaller variations in the speed of sound. Therefore, the results are presented in terms of the following nondimensionalized variables (denoted by the tilde):

$$\tilde{x} = x/d_c \tag{1}$$

$$\tilde{u} = u_0/a_0 \equiv M \tag{2}$$

$$\tilde{t} = a_0 t/d_c \tag{3}$$

where d_c is the diameter of the case.

Instrumentation and Preliminary Data Reduction

Six fast-response pressure transducers (Entran model EPI-080, 34.5-kPa range, 120-kHz natural frequency) were flush mounted in the inlet, on both the casing and the hub. The transducers were located at four axial stations between the pulse generator and the compressor, as indicated in Fig. 3 (stations 1–4). The circumferential location of all transducers was 36 deg clockwise from top dead center. A 12-bit, 1-MHz throughput data acquisition board (resolution approximately equal to 17 Pa) was used to acquire the high-speed data. All dynamic data were digitized at 100 kHz per channel, then were reduced by the respective transducer sensitivities, and were filtered with a low-pass digital filter with pass and cutoff frequencies of 1.5 and 2.0 kHz, respectively, to remove the compressor noise (typically, 7–9 kHz).

Data Reduction: Signal Extraction

A sample data set was selected to illustrate the signal extraction procedure. This data set is representative of any number of runs with the engine operating near the operating line. The corrected speed, overall pressure ratio, VIGV setting Γ, and inlet Mach number were 18,750 rpm, 2.45, 24.8 deg, and 0.17, respectively.

Figures 3a–3d show the reduced and filtered data segments at the four axial stations between the bump and the compressor. In considering these pressure histories, it is helpful to consult the x–t diagram of Fig. 2. The time traces in Fig. 3 correspond to data taken along vertical lines in Fig. 2 at the axial stations 1–4. Figure 2 shows that pulses moving in opposite directions are superimposed in certain regions of the x–t diagram. When a given transducer is simultaneously exposed to two pulses, the signal becomes complex, and the structures of the contributing pulses are not readily recognizable.

The U2 reflection of the D1 pulse from the compressor face is evident in Figs. 3b and 3c (stations 2 and 3). In Fig. 3d (station 4), the reflected and incident pulses (D1 and U2) overlap between $\tilde{t} = 2$ and 6.

Figure 3 shows the pressure–time signal measured at stations 1 and 4. The signal at station 1 is dominated by the incident pulse (D1) whereas the signal at station 4 contains the incident pulse and reflection (U2) superimposed. Because the D1 pulse propagates downstream at a known speed $(u_0 + a_0)$ without changing shape, the reflected pulse can be determined by subtracting the (suitably time shifted) D1 pulse from the measured total signal (superimposed D1 and U2 pulses). The signal at station 3 was unchanged, and the time shift for the trace measured at station 1 is given as

$$(\Delta\tilde{t})_{1\to 3} = \frac{\tilde{x}_3 - \tilde{x}_1}{a_0 + u_0} = \frac{\tilde{x}_3 - \tilde{x}_1}{a_0(1 + M_0)} \tag{4a}$$

The same procedure can be applied to the signal at station 4 using a time shift of

$$(\Delta\tilde{t})_{1\to 4} = \frac{\tilde{x}_4 - \tilde{x}_1}{a_0 + u_0} = \frac{\tilde{x}_4 - \tilde{x}_1}{a_0(1 + M_0)} \tag{4b}$$

i.e., the magnitude of the shift is equal to the planar wave propagation time from station 1 to station 3 or 4. The wave speed was calculated independently of the high-speed data from time-mean measurements of M_0 and T_0.

Figure 4 shows the U2 pulses extracted from the superimposed signals at stations 3 and 4 from the transducers on the hub and case at each station by using this method. The waveforms shown in Fig. 4 were edited by replacing the unwanted portions of each signal, i.e., reflections from the bellmouth with zeros.

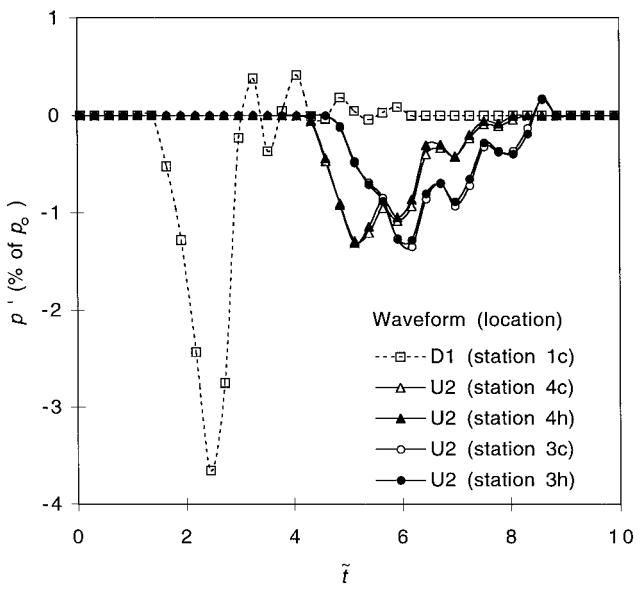

Fig. 4 Edited D1 and U2 pulses.

Reflection Characteristics

Figure 4 shows that the reflection U2 is predominantly an expansion wave, just as its stimulus, D1. However, U2 has a much lower peak amplitude (for this example, 36% of the D1 pulse peak amplitude) but has a duration that is 2.25 longer than the main expansion part of the incident disturbance. This is a strong indication that the downstream moving pulse generates significant reflections from not only the first stage, but also from successive blade rows as it propagates through the compressor.

The compressor rotor and stator vanes on the T58 compressor are not swept and have only a moderate twist; therefore, no major radial variations were expected in the reflection. Figure 4 shows the reflections measured at the hub and case at stations 3 and 4, and indeed the signals (at each station) are nearly identical.

Characterizing the reflection with simple amplitude coefficients was found to be inadequate because the reflection has markedly different shape and duration as compared to the incident pulse. This problem was resolved by adapting a frequency-domain method to provide a complete description of the reflection process.

Frequency-Domain Analysis

Frequency-domain analysis is commonly used in acoustics to determine the complex reflection or transmission coefficients and/or the acoustic impedances of various materials.[36] Details can be found in numerous textbooks and articles and will not be included here. The requisite procedures are also detailed in Ref. 37. The impulse method has been used to find the response characteristics of many types of duct terminations such as: pipe mufflers,[38] duct-nozzle systems,[39] and duct-orifice plate systems.[40]

The method assumes that the input and output functions are linearly related, which is a very reasonable assumption for the acoustic disturbances considered in this work. Given the time histories of the incident and reflected pulses, the transfer functions can be readily calculated with commercial data analysis software (National Instruments LabVIEW software was used).

Given the time histories of the incident and reflected pulses, a transfer function ($H[f]$) can be readily calculated as

$$H[f] = Z[f]/\,Y[f] \tag{5}$$

where $Z[f]$ is the Fourier transform of the reflected pulse signal U2(t) and $Y[f]$ is the Fourier transform of the incident pulse time history D1(t). The transfer function is a complex function that can be represented as

$$H[f] = |H[f]|e^{-i\phi[f]} \tag{6}$$

where $|H[f]|$ is the absolute value and $\phi[f]$ is the phase angle (both are functions of frequency).

In the context of this application, the transfer function is a frequency-resolved reflection coefficient that describes the ratio of the reflected to incident amplitudes and the phase shift occurring in the reflection. The absolute value of $H[f]$ (amplitude ratio) will be denoted $R[f]$.

The frequency can be scaled in a manner analogous to that used for the primitive variables to yield

$$\tilde{f} = f d_c / a_0 \tag{7}$$

A frequency of 1000 Hz corresponds to a nondimensional frequency of 0.7586, assuming a standard, sea-level temperature of 288.14 K.

Power Spectral Densities of D1 and U2

Before evaluating the transfer function, the power spectral densities (PSD) of the D1 and U2 pulses were computed to determine the bandwidth of interest. The power spectra are normalized with respect to the maximum value contained in the incident pulse spectrum. For the D1 pulse, the bulk of the energy is contained below a scaled frequency of 0.75 (1000 Hz), whereas the majority of energy in the U2 pulse is contained in scaled frequencies below 0.30 (400 Hz). At a scaled frequency of 0.75, the PSD of the flow noise

is equal to the PSD of the U2 pulse, i.e., the energy content in the reflected pulse is negligible. Therefore, transfer functions will be presented for scaled frequencies up to 0.75.

Phase Angle Conversion into a Reflection Location

The dependence of the phase angle on frequency is not easily related to a physical quantity. However, $\phi[\tilde{f}]$ divided by $2\pi f$ has the units of seconds and corresponds to a time delay ($\tau[\tilde{f}]$) (Ref. 41). In our application, the time delay is equivalent to the D1 pulse propagation time from station 1 to the compressor plus the propagation time of the U2 reflection from the compressor to station 3 or 4. Assuming that M_0 and a_0 are constant through the compressor (an appropriate first-order approximation) and have the same values as in the inlet, then the axial reflection plane ($\xi[\tilde{f}]$) within the engine can be evaluated as

$$\xi[\tilde{f}] = \tfrac{1}{2}\left[\tau[\tilde{f}]a_0\left(1 - M_0^2\right) + x_1(1 - M_0) + x_i(1 + M_0)\right] \quad (8)$$

where x_i is the axial location, i.e., station 3 or 4, of the transducer used to define the reflection. The scaled axial reflection plane is defined as

$$\tilde{\xi}[\tilde{f}] = \xi[\tilde{f}]/d_c \quad (9)$$

Where a positive $\tilde{\xi}[\tilde{f}]$ describes a reflection downstream of the reference reflection plane, i.e., from the compressor interior.

Parametric Study

This experiment has four parameters that can be independently varied: incident pulse strength, compressor pressure ratio, Mach number M_0, and variable vane geometry, i.e., the stagger angle of the VIGVs and stages 1–3 variable stators. The variable geometry will be represented by the stagger angle of the VIGVs. Note that the variable geometry is gang controlled, and an increase in the stagger angle of the VIGVs is accompanied by an increase in the stagger angles for all three variable stators.

For brevity, the results discussed in the following sections (see Figs. 5–8) are presented in terms of the amplitude ratio (R[$\tilde{f}$]) and scaled reflection location ($\tilde{\xi}[\tilde{f}]$). All of the curves shown represent the mean computed from the four transfer functions available in each run (one pair at each station 3 and 4). Because the overall repeatability in the frequency domain was found to be satisfactory, one run will be used to represent the various conditions.

Effect of Pulse Amplitude

A study was conducted to determine the effect of the incident pulse strength on the reflection, with the amplitude of D1 varying

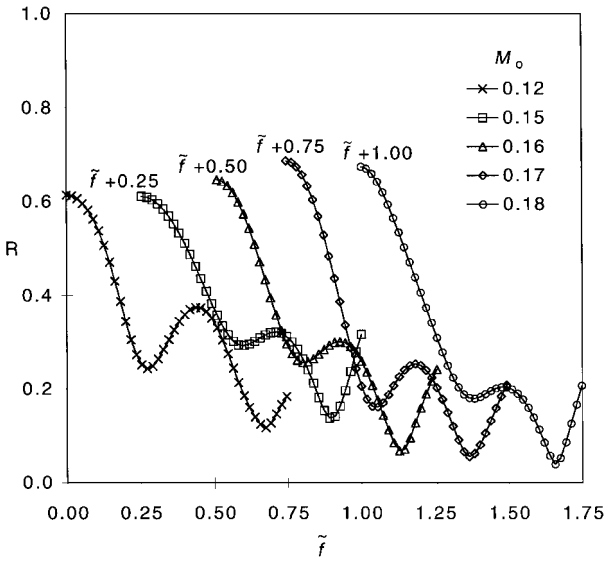

Fig. 5a Amplitude ratio *R*, for Γ = 19.8 deg.

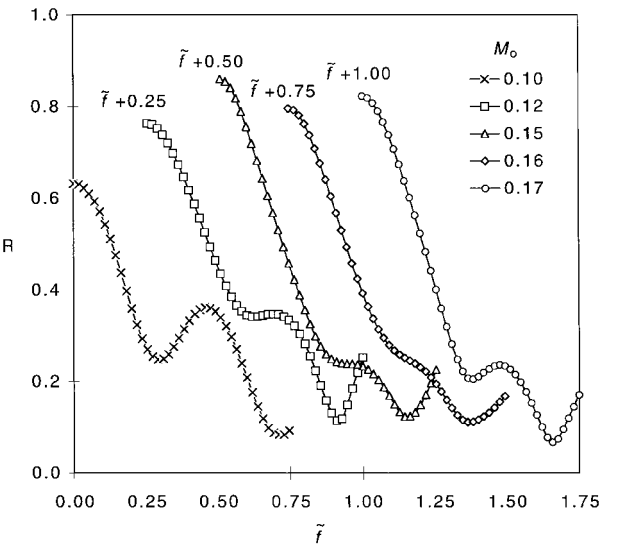

Fig. 6a Amplitude ratio *R*, for Γ = 24.8 deg.

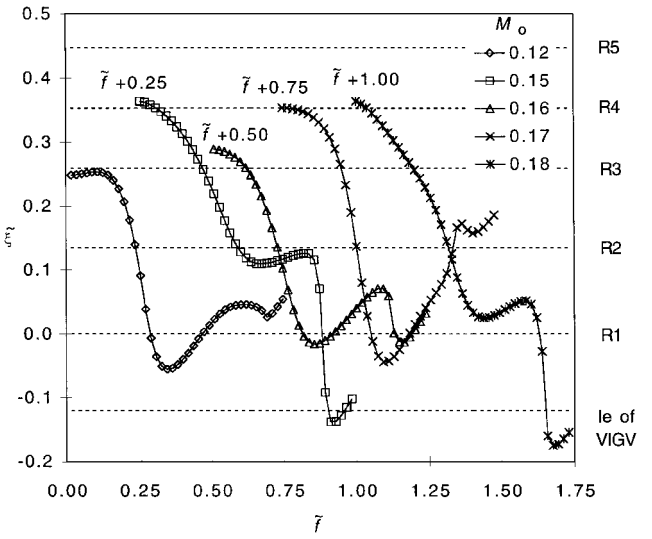

Fig. 5b Reflection location $\tilde{\xi}$, for Γ = 19.8 deg.

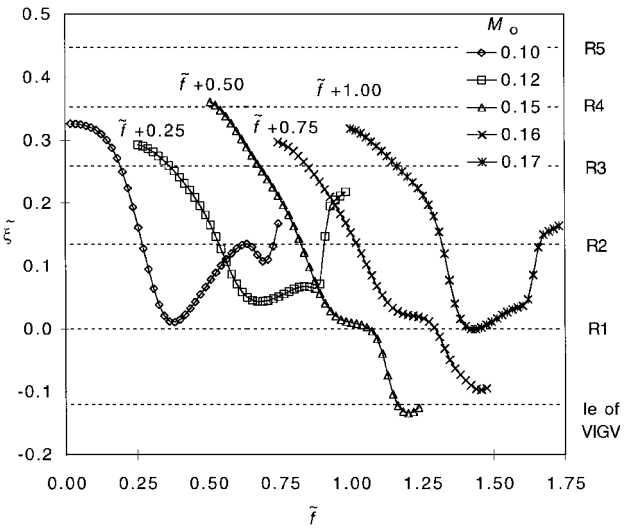

Fig. 6b Reflection location $\tilde{\xi}$, for Γ = 24.8 deg.

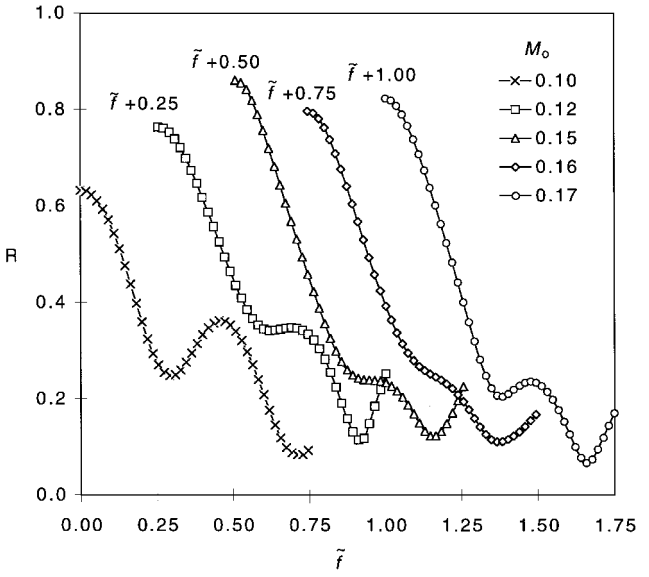

Fig. 7a Amplitude ratio R, for $M_0 = 0.16$.

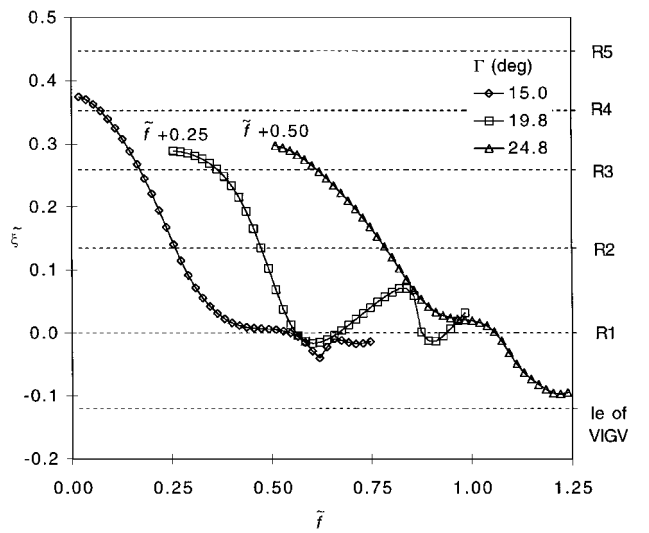

Fig. 7b Reflection location $\tilde{\xi}$, for $M_0 = 0.16$.

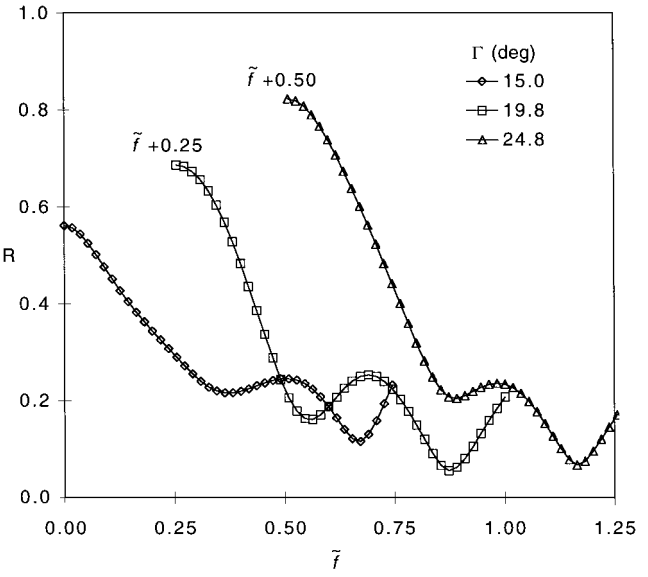

Fig. 8a Amplitude ratio R, for $M_0 = 0.17$.

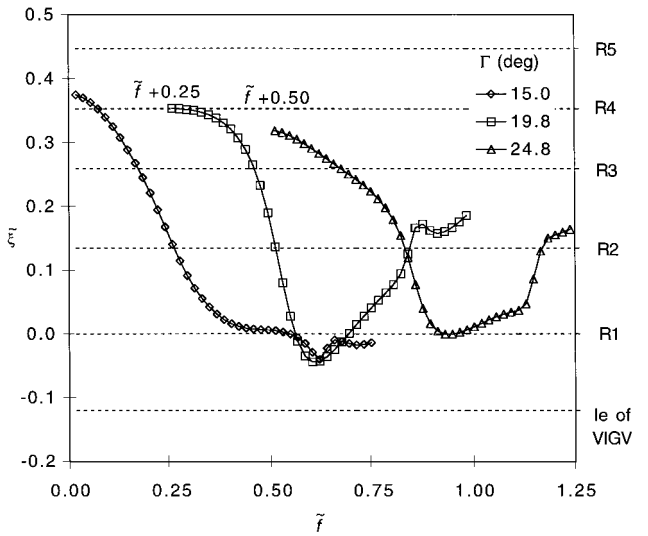

Fig. 8b Reflection location $\tilde{\xi}$, for $M_0 = 0.17$.

from 3.3 to 4.5% of p_0. The strength of the incident pulse was shown not to affect the transfer function to an appreciable degree. The variations are of the same magnitude as the repeatability of the tests.

The experimental results agree with a computational analysis performed by Paynter.[30] Paynter varied the incident disturbance amplitude from 1 to 10% of p_0 and reported no sizable influence on the ratio of the reflected to incident peak amplitudes. The experimental results and Paynter's computational results indicate that the reflection process is linear for the range of incident pulse amplitudes considered in this work.

Effect of Compressor Pressure Ratio

In a second series of tests, the overall compressor pressure ratio was varied from 1.28 to 2.04. The transfer functions were nearly identical for all compressor pressure ratios, at any given rotational speed. This result is not surprising because the reported pressure ratios resulted in a stage pressure ratio (assuming the same pressure per stage for all stages) between 1.025 and 1.074 (a 5% difference).

For all of the runs reported in the following sections, the compressor was loaded to perform slightly below the operating line, a selection based solely on the need to conserve the turbine supply air.

Effect of Mach Number

In the third series of tests, Γ was held constant at settings of 15.0, 19.8, 24.8, 29.9, and 31.7 deg, while the Mach number (controlled through the compressor speed) was parametrically varied. Figures 5a and 6a show the amplitude ratios for selected Γ settings of 19.8 and 24.8 deg, respectively. In Figs. 5a and 6a, data are given parametrically for several constant values of Mach numbers.

For all of the data presented in Figs. 5a and 6a, the amplitude ratio vs the scaled frequency exhibits the characteristic of a low-pass filter. This is consistent with the observation that all U2 reflections were shown to be considerably longer in duration than the D1 incident pulses.

Using the amplitude ratio at a scaled frequency of 0, i.e., dc component as a crude measure of the strength of the reflection, permits the following observation: small increases in the Mach number generally result in small increases the strength of the reflection.

The phase information for the transfer functions used to create Figs. 5 and 6 was converted into a time delay, which was then converted into an axial reflection, via Eq. (8). The results are shown in Figs. 5b and 6b, which are companion plots for Figs. 5a and 6a.

All of the scaled reflection location curves show that the equivalent reflection location occurs within the compressor, for scaled frequencies below 0.6 (approximately equal to 800 Hz, where the majority of the energy is contained).

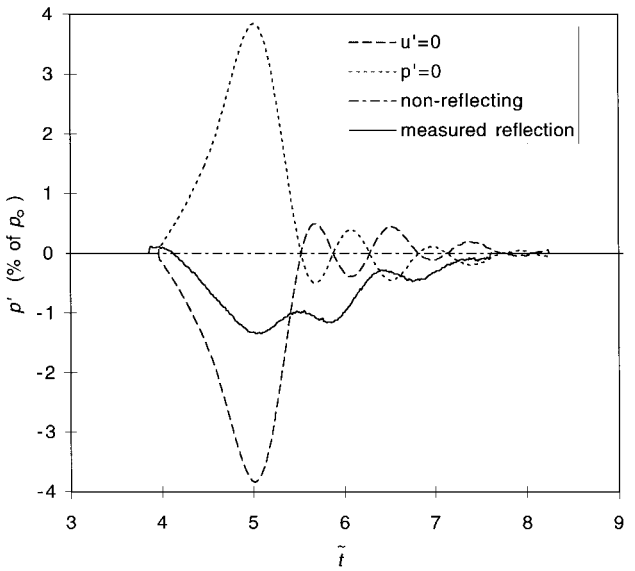

Fig. 9 Comparison of constant parameter and nonreflecting boundary conditions to data.

Effect of Variable Geometry Γ

Figures 7 and 8 show the amplitude ratios and reflection location for constant Mach numbers of 0.16 and 0.17.

Figures 7a and 8a show that increasing Γ results in higher amplitude ratios at low frequencies, where the majority of the U2 energy is contained. This was expected because increasing the stagger angle of the variable geometry increases the total blade area projected onto a plane normal to the axis, i.e., the pulse "sees" more surface it can reflect from.

Figures 7b and 8b show the depth of the reflection increases with decreasing Γ, at least for corrected frequencies below 0.30 (400 Hz). This appears reasonable because lower Γ values reflect less of the D1 pulse in the front stages of the compressor, resulting in a larger part transmitted to the interior stages of the compressor, thus producing stronger reflections at larger $\tilde{\xi}[\tilde{f}]$ values.

Comparison of Results with Current Compressor-Face Boundary Conditions

Figure 9 compares the reflection shown in Fig. 4 (station 4, on the case) to those predicted by the constant velocity and the constant pressure boundary conditions, which appear to be the most commonly employed. It is clear that these conditions invariably predict a reflection that has the same duration and the same magnitude as the incident pulse. The constant pressure boundary condition predicts a reflection whose sign is opposite to that of the incident pulse, i.e., a compression pulse in the present situation. Clearly, the constant pressure condition does not predict even the sign of the reflection correctly. The constant velocity condition predicts a same sign reflection (an expansion pulse in our case), but the predicted magnitude differs substantially from the experimental findings.

In terms of the frequency-resolved reflection coefficient, the constant velocity boundary condition implies a gain of one and a phase angle of zero, i.e., the reflection occurs at the axial position at which it is imposed, for all frequencies. The constant pressure condition implies a gain of negative unity with a phase angle of zero, for all frequencies. Figures 5–8 show that neither is a realistic approximation of the data.

Implementation of Frequency-Domain Boundary Conditions in Time-Domain Codes

The present work is confined to the presentation of experimental information. The spectral format used to present the data is both convenient and complete, but cannot be readily incorporated into computational codes that are based on time-domain representations. If the information offered here is to be employed for practical use, then an appropriate numerical formulation must be incorporated into CFD codes.

The implementation of time-domain boundary conditions that are practical equivalents of frequency-domain (impedance) boundary conditions have been recently studied in computational aeroacoustics by Ozyoruk and Long[42,43] and Tam and Auriault.[44] Using an approach similar in nature, it is believed that the data generated in this study could be implemented as an outflow boundary condition in a CFD code.

Conclusions

Measurements were made of a transient process in which an acoustic expansion pulse propagates to and is reflected from an operating axial, multistage compressor. The wave propagation occurs in a constant-area, annular inlet. The incident pulse is free of vorticity and entropy variations. It is also nearly planar, has a duration of approximately 1 ms, and has a peak amplitude of approximately 4% of the mean static pressure.

The reflections were found to be expansion pulses also, with amplitudes much less and durations much longer than those of the incident pulse. The long duration is probably caused by the incident pulse penetrating the first three or four stages and creating partial reflections from each.

Frequency-domain analysis was used to characterize the results in terms of transfer functions. This approach provides a fairly complete description of the reflection process.

The principal factors affecting the transfer functions were found to be the VIGV setting, i.e., stagger angle, and the axial Mach number in the duct. The amplitude of the reflection was shown to increase both with increasing Mach number and with increasing VIGV stagger angle. The transfer function was not significantly affected by changing the incident pulse strength or by varying the compressor overall pressure ratio (loading).

Reflections predicted by two currently customary compressor-face boundary conditions (constant pressure and constant velocity) were compared to a measured reflection. The predictions differed sharply from the experimental data, indicating that a review and revision of current practices in specifying outflow conditions for unsteady inlet flow computations is warranted.

Acknowledgments

This program has been funded in part by the University of Cincinnati and in part by the Ohio Board of Regents, through the Ohio Eminent Scholar Program. After 1 January 1997, support has been provided by John H. Glenn Research Center at Lewis Field, with Gary Cole acting as Technical Officer. The authors would like to thank Gerald Paynter of The Boeing Company and Gary Cole and Joungkee Chung of John H. Glenn Research Center at Lewis Field for numerous enlightening discussions concerning compressor-face boundary conditions issues. John Slater of John H. Glenn Research Center at Lewis Field helped in the design of the experiment by supplying invaluable computational predictions of the pulse generating process. The authors are greatly indebted to Russell DiMicco, without whose dedicated support this project would not have been possible. Jay Kim of the University of Cincinnati has advised the authors concerning the use of frequency-domain analysis methods. The assistance provided by John Vasquez in setting up the experiment and operating the compressor rig is greatly appreciated.

References

[1]Mattingly, J. D., Heiser, W. H., and Daley, D. H., *Aircraft Engine Design*, American Inst. of Aeronautics and Astronautics, New York, 1987, p. 381.

[2]Domack, C. S., "A Preliminary Investigation of Inlet Unstart Effects on a High-Speed Civil Transport Concept," AIAA Paper 91-3327, Sept. 1991.

[3]Clark, L. T., "Dynamic Response Characteristics of a Mixed Compression Supersonic Inlet as a Part of a Larger System," AIAA Paper 95-0036, Jan. 1995.

[4]Chung, J., "Numerical Simulation of a Mixed-Compression Supersonic Inlet Flow," AIAA Paper 94-0583, Jan. 1994.

[5]Chung, J., and Cole, G. L., "Comparison of Compressor Face Boundary Conditions for Unsteady CFD Simulations of Supersonic Inlets," AIAA Paper 95-2627, July 1995.

[6]Decher, R., Mayer, D. W., and Paynter, G. C., "On Supersonic Inlet-Engine Stability," AIAA Paper 94-3371, July 1994.

[7]Mayer, W. D., and Paynter, G. C., "Prediction of Supersonic Inlet Unstart Caused by Freestream Disturbances," *AIAA Journal*, Vol. 33, No. 2, 1995, pp. 256–275.

[8]Mayer, W. D., and Paynter, G. C., "Boundary Conditions for Unsteady Supersonic Inlet Analyses," *AIAA Journal*, Vol. 32, No. 6, 1994, pp. 1200–1206.

[9]Paynter, G. C., Mayer, D. W., and Tjonneland, E., "Flow Stability Issues in Supersonic Inlet Flow Analyses," AIAA Paper 93-0290, Jan. 1993.

[10]Saunders, J. D., and Keith, T. G., "Results From Computational Analysis of Mixed Compression Supersonic Inlet," AIAA Paper 91-2581, 1991.

[11]Numbers, K., and Hamed, A., "Development of a Coupled Inlet-Engine Dynamic Analysis Method," AIAA Paper 97-2880, July 1997.

[12]Sugiyama, Y., Tabakoff, W., and Hamed, A., "J85 Surge Transient Simulation," *Journal of Propulsion and Power*, Vol. 5, No. 3, 1989, pp. 375–381.

[13]Cole, G. L., "Atmospheric Effects on Inlets for Supersonic Cruise Aircraft," AIAA Paper 77-874, July 1977.

[14]Wasserbauer, J. F., and Whipple, D. L., "Experimental Investigation of the Dynamic Response of a Supersonic Inlet to External and Internal Disturbances," NASA TM X-1648, Sept. 1968.

[15]Baumbick, R. J., Wallhagen, R. E., Neiner, G. H., and Batterton, P. G., "Dynamic Response of Mach 2.5 Axisymmetric Inlet with 40 Percent Supersonic Internal Area Contraction," NASA TM X-2833, July 1973.

[16]Sanders, B. W., "Dynamic Response of a Mach 2.5 Axisymmetric Inlet and Turbojet Engine with a Poppet-Valve-Controlled Inlet-Stability Bypass System when Subjected to Internal and External Airflow Transients," NASA TP-1531, Jan. 1980.

[17]Wasserbauer, J. F., "Dynamic Response of a Mach 2.5 Axisymmetric Inlet with Engine or Cold Pipe and Utilizing 60 Percent Supersonic Internal Area Contraction," NASA TN D-5338, July 1969.

[18]Brimelow, B., Collins, T. P., and Pfefferkorn, G. A., "Engine Testing in a Dynamic Environment," AIAA Paper 74-1198, Oct. 1974.

[19]Melick, H. C., "Analysis of Inlet Flow Distortion and Turbulence Effects on Compressor Stability," NASA TR CR-114577, March 1973.

[20]Das, D. K., and Trippi, A., "Effects of Inlet Pressure Fluctuations on Axial Flow Compressors," *Journal of Propulsion and Power*, Vol. 5, No. 1, 1989, pp. 72–81.

[21]Kurkov, A. P., Soeder, R. H., and Moss, J. E., "Investigation of the Stall Hammershock at the Engine Inlet," *Journal of Aircraft*, Vol. 12, No. 4, 1975, pp. 198–204.

[22]Marshall, F. L., "Prediction of Inlet Duct Overpressures Resulting from Engine Surge," *Journal of Aircraft*, Vol. 10, No. 5, 1973, pp. 274–278.

[23]Ferri, A., and Nucci, L. M., "The Origin of Aerodynamic Instability of Supersonic Inlets at Subcritical Conditions," NACA RM L50K30, Jan. 1951.

[24]Kovasznay, L. S. G., "Turbulence in Supersonic Flow," *Journal of the Aeronautical Sciences*, Vol. 20, No. 10, 1953, pp. 657–675.

[25]Reynolds, G. G., Vier, W. F., and Collins, T. P., "An Experimental Evaluation of Unsteady Flow Effects on an Axial Compressor—P3 Generator Program," U.S. Air Force Aero Propulsion Lab. Technical Rep. AFAPL-TR-73-43, Wright–Patterson AFB, OH, July 1973.

[26]Peacock, R. E., "An Experimental Study of Pulsating Flow in a Three-Stage Axial Flow Compressor," *Proceedings of the Winter Annual Meeting*, American Society of Mechanical Engineers, San Francisco, CA, Dec. 1978, pp. 185–191.

[27]Kaji, S., and Okazaki, T., "Propagation of Sound Waves Through a Blade Row: I. Analysis Based on the Semi-Actuator Disk Theory," *Journal of Sound and Vibration*, Vol. 11, No. 3, 1970, pp. 339–353.

[28]Kaji, S., and Okazaki, T., "Propagation of Sound Waves Through a Blade Row: II. Analysis Based on the Acceleration Potential Method," *Journal of Sound and Vibration*, Vol. 11, No. 3, 1970, pp. 355–370.

[29]Paynter, G. C., Clark, L. T., and Cole, G. L., "Modeling the Response from a Cascade to an Upstream Acoustic Disturbance," AIAA Paper 98-0953, Jan. 1998.

[30]Paynter, G. C., "Response of a Two-Dimensional Cascade to an Upstream Disturbance," *AIAA Journal*, Vol. 35, No. 3, 1997, pp. 434–440.

[31]Freund, D. D., "Experimental Exploration of Compressor-Face Boundary Conditions for Unsteady Inlet Flow Computations," Ph.D. Dissertation, Dept. of Aerospace Engineering and Engineering Mechanics, Univ. of Cincinnati, Cincinnati, OH, Dec. 1997.

[32]Freund, D., and Sajben, M., "Reflection of Large Amplitude Acoustic Pulses from an Axial Flow Compressor," AIAA Paper 97-2879, July 1997.

[33]Freund, D., and Sajben, M., "Experimental Investigation of Outflow Boundary Conditions Used in Unsteady Inlet Flow Computations," AIAA Paper 97-0610, Jan. 1997.

[34]Freund, D., and Sajben, M., "Compressor-Face Boundary Condition Experiment: Generation of Acoustic Pulses in Annular Ducts," AIAA Paper 96-2657, July 1996.

[35]Sajben, M., and Freund, D. D., "Experimental Exploration of Compressor-Face Boundary Conditions for Unsteady Inlet Flow Computations," AIAA Paper 95-2886, July 1995.

[36]Chung, J. Y., and Blaser, D. A., "Transfer Function Method of Measuring In-Duct Acoustic Properties. Part II, Experiment," *Journal of the Acoustic Society of America*, Vol. 68, No. 3, 1980, pp. 914–921.

[37]"Standard Test Method for Impedance and Absorption of Acoustic Materials Using a Tube, Two Microphones, and a Digital Frequency Analysis System," ASTM Standard: E1050-98, American Society for Testing and Materials, West Conshohocken, PA, May 1998.

[38]Singh, R., and Katra, T., "Development of an Impulse Technique for Measurement of Muffler Characteristics," *Journal of Sound and Vibration*, Vol. 56, No. 2, 1978, pp. 279–298.

[39]Salikuddin, M., and Mungur, P., "Acoustic Radiation Impedance of Duct-Nozzle System," *Journal of Sound and Vibration*, Vol. 86, No. 4, 1981, pp. 497–522.

[40]Salikuddin, M., and Plumblee, H. E., "Low Frequency Sound Absorption of Orifice Plates and Nozzles," AIAA Paper 80-0991, June 1980.

[41]Bendat, J. S., and Piersol, A. G., *Engineering Applications or Correlation and Spectral Analysis*, Wiley, New York, 1980, p. 67.

[42]Ozyoruk, Y., and Long, L., "A Time-Domain Implementation of Surface Acoustic Impedance Condition with and without Flow," AIAA Paper 96-1663, May 1996.

[43]Ozyoruk, Y., and Long, L., "Impedance Boundary Conditions for Time-Domain Computational Aeroacoustics Methods," AIAA Paper 97-0021, Jan. 1997.

[44]Tam, C. K. W., and Auriault, L., "Time-Domain Impedance Boundary Conditions for Computational Aeroacoustics," *AIAA Journal*, Vol. 34, No. 5, 1996, pp. 917–923.